

GRS 1915+105 as a Galactic Analog of a Fanaroff-Riley II Quasar

Brian Punsly¹

and

Jérôme Rodriguez²

ABSTRACT

We study the long term time averaged kinetic luminosity, \overline{Q} , of the major flares of the Galactic microquasar GRS 1915+105 and the relationship to the intrinsic X-ray (bolometric) luminosity, L_{bol} , and scale it to that of a complete sample of SDSS/FIRST FR II quasars. If the scale invariance hypothesis for black holes (BHs) holds then we show that the expected distribution in the \overline{Q} - L_{bol} scatter plane of GRS 1915+105 is consistent with FR II quasars for distances $D = 10.7 - 11$ kpc. We compare the specific values of kinetic luminosity and L_{bol} during flares of GRS 1915+105 to that predicted by several 3-D MHD simulations of BH accretion flows with relativistic ejections. If FR II quasars are a scaled up version of GRS 1915+105, the data are consistent with numerical models when they contain an ergospheric disk jet and the BH spin is $a/M = 0.99$ or $a/M = 0.998$ (we estimate $a/M > 0.984$). In the framework of scale invariance of BHs, our results may imply that FR II quasars also hold rapidly rotating BHs.

Subject headings: Black hole physics — magnetohydrodynamics (MHD) — galaxies: jets—galaxies: active — accretion, accretion disks

1. Introduction

The black hole candidate GRS 1915+105 is well known for launching superluminal radio flares out to large distances at a much larger rate than any other Galactic object (Mirabel and Rodriguez 1994; Fender et al 1999; Dhawan et al 2000). The X-ray luminosity

¹1415 Granvia Altamira, Palos Verdes Estates CA, USA 90274 and ICRANet, Piazza della Repubblica 10 Pescara 65100, Italy, brian.punsly1@verizon.net or brian.punsly@comdev-usa.com

²Laboratoire AIM, CEA/DSM-CNRS-Université Paris Diderot, IRFU SAp, F-91191 Gif-sur-Yvette, France.

of GRS 1915+105 is one of the highest of any known Galactic black hole (BH) candidate (Done et al 2004). The existence of both relativistic outflows and high continuum luminosity make it tempting to speculate that GRS 1915+105 might be a scaled down version of a radio loud quasar. This is of particular importance because the time scales for radio evolution are reduced from the AGN (active galactic nuclei) time scales by many orders of magnitude. Thus, unlike quasars, it is in principle possible to see the details of the connection between the putative accretion flow (X-ray luminosity) and the superluminal jet launching mechanism.

In this article, the idea of GRS 1915+105 as a scaled down FR(Fanaroff-Riley) II quasar is explored. The long term time averaged power of the relativistic major flares in GRS 1915+105, \overline{Q} , and the luminosity associated with viscous dissipation in the accretion flow, L_{bol} , are re-scaled in order to compare and contrast with the distribution of \overline{Q} and L_{bol} of a complete sample of FR II quasars. These efforts are rendered credible by the recent study of the power required to launch individual major flares and their accretion state (intrinsic X-ray luminosity or bolometric luminosity, L_{bol}) just hours and minutes before ejection and during the brief 1 to 7 hour ejection event (Punsly and Rodrgiuez (2013), PR13 hereafter). The relevant results from PR13 that are required to perform this re-scaling are indicated in Section 2. In Section 3, this is compared to FR II quasars. In Section 4, the results of Sections 2 and 3 are considered in the context of numerical simulations of 3-D MHD (magnetohydrodynamic) accretion around spinning BHs.

2. Estimating the Energy Output from Relativistic Ejecta in GRS 1915+105

It was determined in Punsly (2012), P12, that knowledge of the time evolution of the spectral shape associated with a changing synchrotron - self absorbed (SSA) opacity, τ , greatly enhances the accuracy of plasmoid energy estimates (constrains the size). The frequency and the width of the spectral peak provide two added pieces of information at each epoch of observation beyond the single epoch spectral index and flux density of the optically thin high frequency tail that is traditionally used to estimate the ejected plasmoid energy. The evolving τ combined with baryon number conservation, energy conservation, synchrotron cooling times and X-ray luminosity were used in P12 to eliminate uncertainty in the energy estimates. Namely, the proton content is minimal and a near minimum energy condition, $E_{\text{min}} \approx m_e c^2$, is shown to occur when the optically thin flux at 2.3 GHz, $S_{\text{thin}}(2.3)$, is near maximum and $\tau \approx 0.1$. In PR13 we assume that the detailed modeling of the time evolution of the flares from P12 can be used as a template for the time evolution of other plasmoids with less supporting data. This determines a set of equations for each flare in PR13 that are solved numerically with 4 inputs, the peak $S_{\text{thin}}(2.3)$, the spectral index of

the optically thin emission, D , and the Doppler factor, δ . Figure 1 is a plot of the plasmoid energy estimated in Table 2 of PR13 as a function of the estimated peak $S_{\text{thin}}(2.3)$ for the major flares that were listed in Table 1 of PR13. Except when noted, a fiducial distance to GRS 1915+105 of $D = 11$ kpc is assumed throughout the manuscript. Unlike Table 2 of PR13, the energy is measured in the observer’s reference frame instead of the plasmoid reference frame. The power law fit in Figure 1 was made with the method of weighted least squares with errors in both variables (Reed 1989). The corresponding power law fit for each D value is used here to estimate flare energy from a single input, the peak $S_{\text{thin}}(2.3)$. The approximately daily 2.3 GHz and 8.3 GHz monitoring with GBI (Green Bank Interferometer) provides a database from 1996 through 2000 of 1967 days (taking account of gaps in coverage) for which one can determine $S_{\text{thin}}(2.3)$. The resulting distributions of major flare energy and number from 1996 through 2000 are plotted in Figure 2.

There are three major sources of uncertainty in the long term cumulative energy, E , from the flares

1. The uncertainty in the estimate of the plasmoid energy
2. The minimal $S_{\text{thin}}(2.3)$ that is indicative of a superluminal ejection
3. Possible short (weak) flares missed in the intra-day gaps in coverage

The stochastic error in the first item is ignored because there are sufficient flares to drive the propagated random error to approximately 0. We consider every plausible value of D and the corresponding dependent δ because of the large systematic uncertainty in δ . In order to estimate δ from D , we assume that the kinematic results from Fender et al (1999) are common to the entire time frame from 1997 to 2000 as evidenced by interferometric observations of multiple flares (Dhawan et al 2000; Miller-Jones et al 2005). The *intrinsic* spectral luminosity is $S_{\text{thin}}(2.3)\delta^{-(3+\alpha)}$. As D is varied from 10.5 kpc to near the maximum kinematically allowed value of 11 kpc, the intrinsic spectral luminosity changes by a factor $\approx (0.31/0.54)^{3.9} = (1/8.7)$ which equates to a reduction of the plasmoid energy by a factor of 5 - 6. Alternatively, the discussions to follow can be phrased in terms of δ instead of D . For item 2, we assume that the weakest flares have a peak $S_{\text{thin}}(2.3) = 30$ mJy since this is the smallest value that can be clearly discerned from a background consisting of core flux variations and previous fading flares. Extrapolating the distributions in Figure 2 to lower cutoffs shows that the total energy output is rather insensitive to the low energy cutoff of the flares - most of the flares are weak, but they carry a small fraction of the total energy output. We estimate the contribution from weak flares in the intra-day gaps and the uncertainty from points 2 and 3 to compute \overline{Q} ,

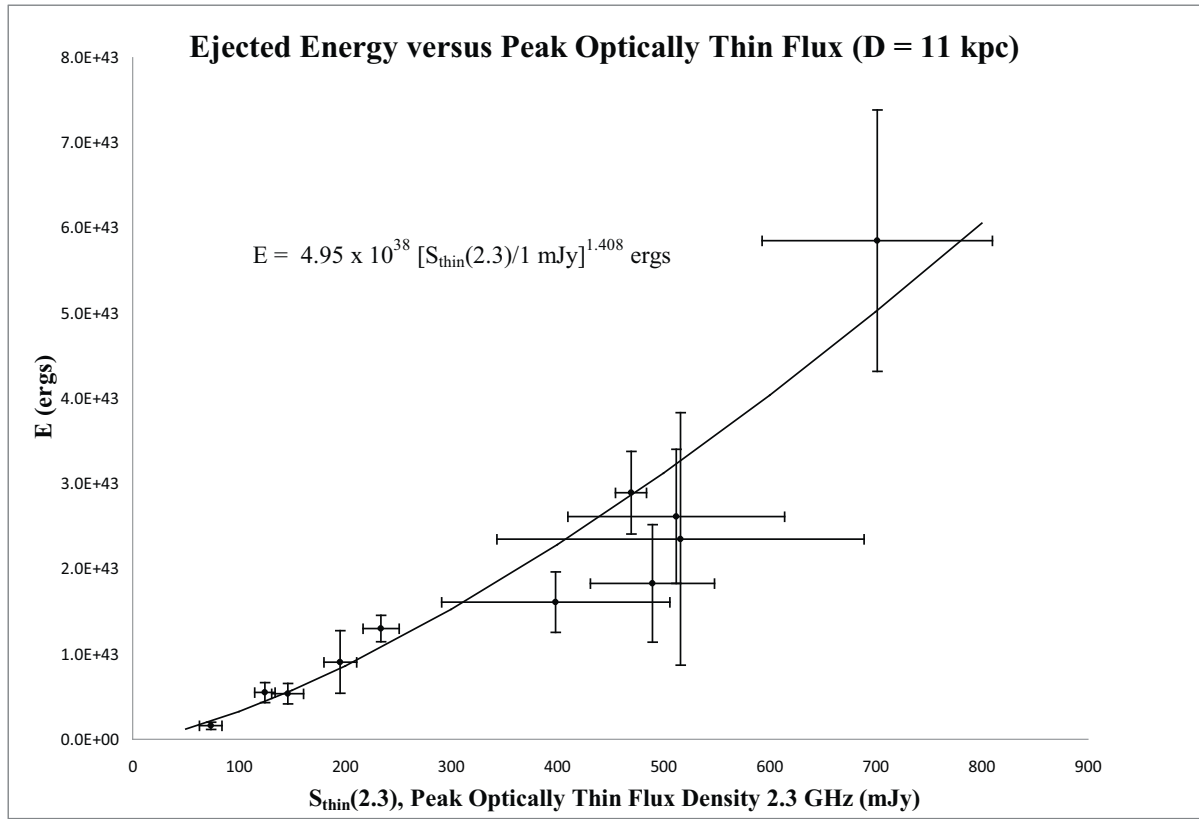


Fig. 1.— This scatter plot of the estimated energy of superluminal ejections from PR13 evaluated in the observer reference frame versus the estimated peak $S_{\text{thin}}(2.3)$

$$\begin{aligned}\overline{Q} &= \frac{\text{cumulative energy of major ejections}}{1967 \text{ days}} \\ &= \frac{1.78 \pm 0.21 \times 10^{45} \text{ ergs}}{1967 \text{ days}} = 1.04 \pm 0.13 \times 10^{37} \text{ ergs/s.}\end{aligned}\tag{1}$$

3. Scaling to a Supermassive Black Hole

In this section, GRS 1915+105 is re-scaled to FR II quasar values of L_{bol} . A complete sample of quasars was created in Punsly and Zhang (2011) using the combined SDSS and FIRST databases. The radio sensitivity was adequate to detect extended emission below the FR I/FR II divide. Thus, a complete distribution of FR II quasars is attained. Furthermore, the \overline{Q} estimates are far more accurate than other treatments of FIRST data in the literature. Radio images were used to subtract the jet emission and core emission on scales less than 20 kpc in order to more accurately determine the optically thin lobe flux density which is the most robust estimator for \overline{Q} (Willott et al. 1999). The blue dots in Figure 3 are the \overline{Q} - L_{bol} scatter plot from the top left frame of Figure 3 in Punsly and Zhang (2011) with the conversion from the integrated optical/UV continuum luminosity to L_{bol} given by Equation (3) of that paper. The L_{bol} estimate is based on flux that is emitted $\sim 10^6 - 10^7$ years after the preponderance of plasma that is responsible for \overline{Q} was ejected from the central engine, based on lobe separation and estimates of lobe advance speeds (Willott et al. 1999). Thus, the epochs are so displaced in time that there need not be a causal connection. In order to compare GRS 1915+105 to the AGN data, one needs to compare \overline{Q} in GRS 1915+105 to L_{bol} at epochs that are not likely to be causally related, i.e. randomly selected from the historical distribution of L_{bol} .

This random data sampling is explored with Monte Carlo simulations. First, we create a distribution of quasar L_{bol} from the SDSS/FIRST data scatter, $f_{\text{quasar}}(L_{\text{bol}})$. Second, the L_{bol} distribution of GRS 1915+105 from PR13 Figure 16 and \overline{Q} from Equation (1) are combined to create a random distribution of $\overline{Q}/L_{\text{bol}}$, $f_{\text{GRS1915}} \left[\log \left(\frac{\overline{Q}}{L_{\text{bol}}} \right) \right]$. Then we create pairs of points representing the re-scaled GRS 1915+105 based on re-scaling L_{bol} to the quasar level. This is accomplished by randomly generating L_{bol} from $f_{\text{quasar}}(L_{\text{bol}})$ then creating \overline{Q} randomly for each L_{bol} from $f_{\text{GRS1915}} \left[\log \left(\frac{\overline{Q}}{L_{\text{bol}}} \right) \right]$. The red dots in Figure 3 represent Monte Carlo simulations of the re-scaled GRS 1915+105 with L_{bol} distributed similarly to the SDSS/FIRST FR II sample. The explicit expressions for the quasar luminosity distribution (the blue dots in Figure 3), $f_{\text{quasar}}(L_{\text{bol}})$, is consistent with a log-normal distribution, Z , with

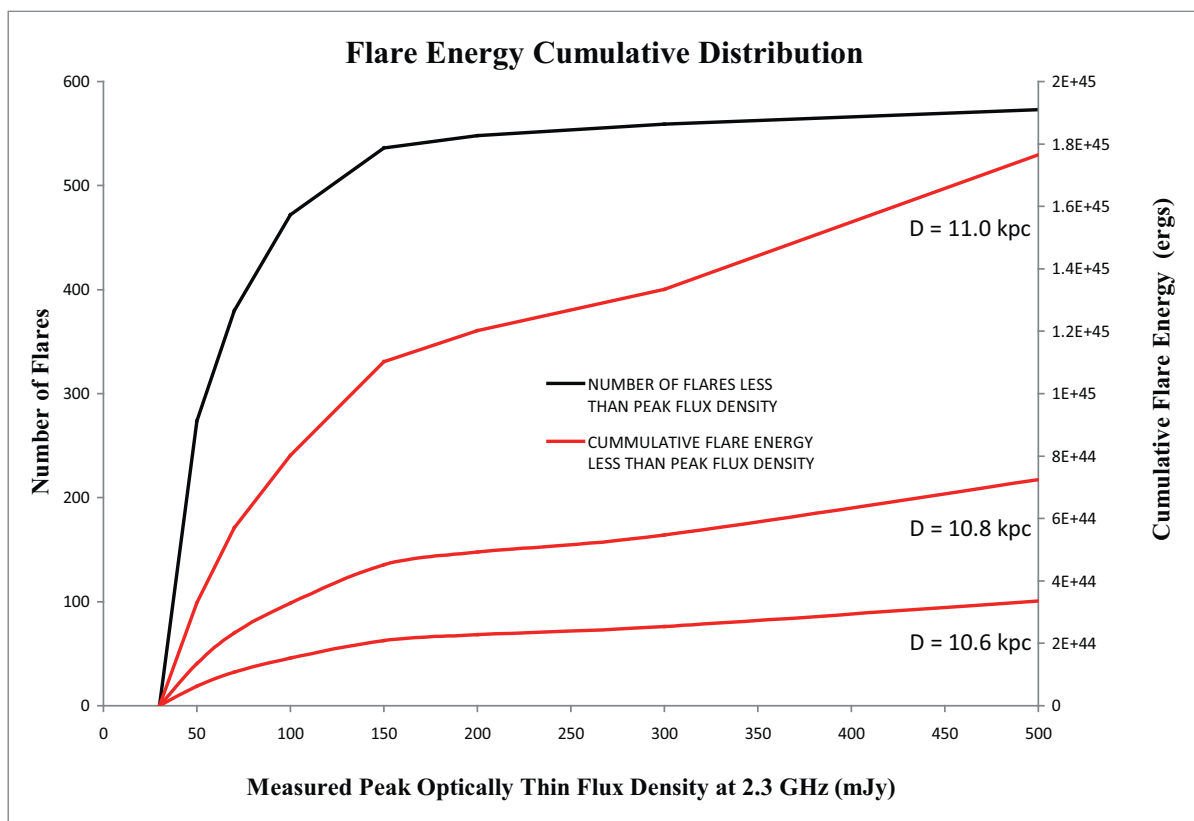


Fig. 2.— The distributions of number and energy ejected in major flares emitted from GRS 1915+105 from 1996 to the end of 2000 (see text for details). The black (red) curve is the cumulative distribution of flare number (energy) in the 1967 days,

a mean logarithm (in units of erg/s) of 45.96 and a standard deviation, 0.29,

$$f_{\text{quasar}}[\log(L_{\text{bol}})] = Z(\mu = 45.96, \sigma = 0.29) . \quad (2)$$

The distribution of L_{bol} for GRS 1915+105 is well described by a log-normal distribution in Figure 16 of PR13

$$f_{\text{GRS1915}}[\log(L_{\text{bol}})] = Z(\mu = 38.73, \sigma = 0.15); , D = 11 \text{ kpc} . \quad (3)$$

From Equations (1) and (3), $\log(\overline{Q}) = -1.71 + \mu[f_{\text{GRS1915}}[\log(L_{\text{bol}})]]$, thus

$$f_{\text{GRS1915}} \left[\log \left(\frac{\overline{Q}}{L_{\text{bol}}} \right) \right] = Z(\mu = -1.71, \sigma = 0.15) , D = 11 \text{ kpc} . \quad (4)$$

Similar expressions for $D < 11$ kpc follow from Table 2 and the methods of PR13 (see Figure 2 also).

For $D = 11$ kpc the 2-D distribution of the re-scaled GRS 1915+105 is clustered near the peak of the quasar distribution. The smaller dispersion of the simulated data is expected because all points are generated by the same central engine as opposed to a variety of central BH masses and enveloping environments that are responsible for the quasar generated scatter. At $D = 10.7$ kpc, $\lesssim 1/2$ of the simulated data is consistent with FR II quasars and at $D = 10.6$ kpc the distributions have become very distinct. Systematic uncertainty is found by comparing the high biased quasar \overline{Q} estimates in Figure 3 from Willott et al. (1999) with the low biased \overline{Q} estimates from the methods of Punsly (2005), that are based on different assumptions. This yields a systematic uncertainty in $\log \overline{Q}$ of 0.38 ± 0.08 , too small to affect the implications of the Monte Carlo simulations. There is very little systematic error in L_{bol} since it is derived from the integrated continuum near the peak of the spectral energy distribution. The systematic uncertainty in \overline{Q} for GRS 1915+105 was discussed in Section 2. The main systematic error in L_{bol} is in the column density, N_H , to the source. From Belloni et al (1997); Munro et al (1999) we expect a systematic error less than a factor of 2 arising from the uncertainty in N_H , too small to affect our conclusions.

4. Results in the Context of Simulations of Black Hole Accretion

We explore the main results from PR13 in the context of numerical simulations

1. Strong flares are launched when L_{bol} is at an elevated level (sometimes approaching the Eddington limit).

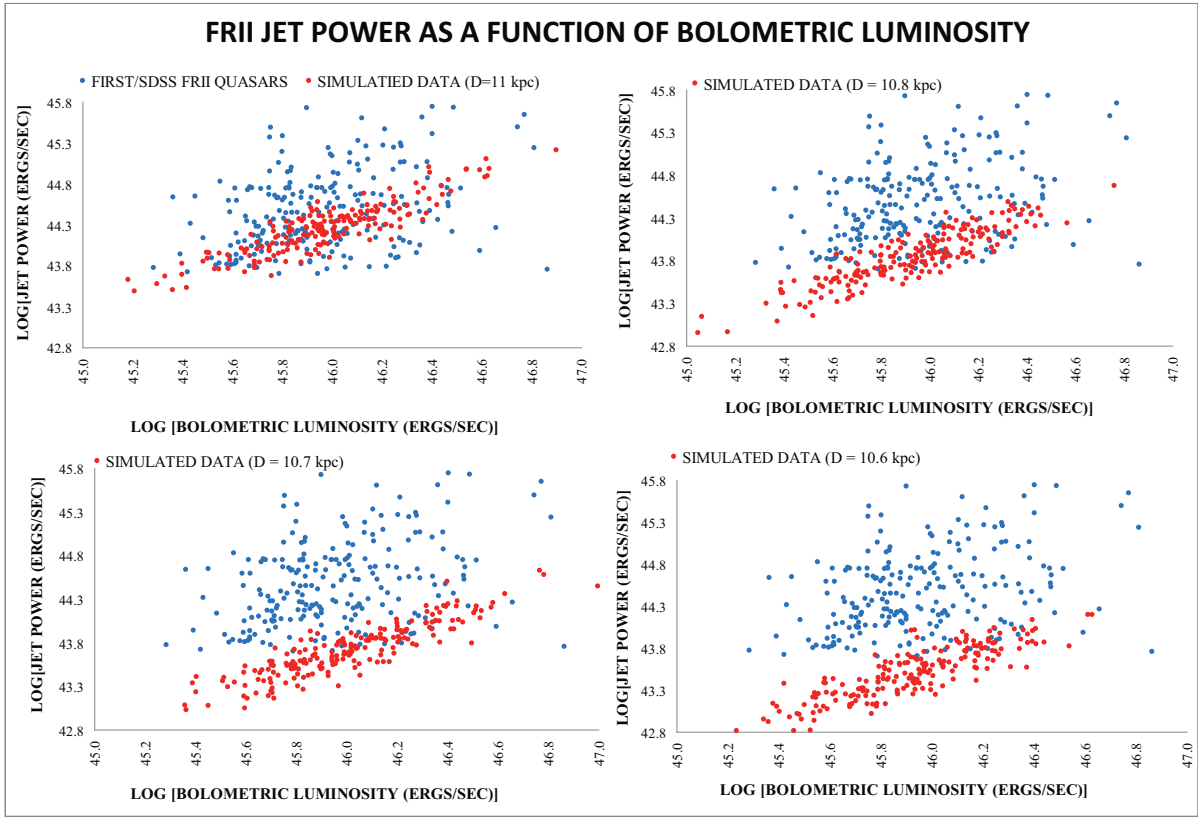


Fig. 3.— Monte Carlo simulations are used to compare the 2-D distribution in the $\overline{Q} - L_{\text{bol}}$ scatter plane for a complete sample of SDSS/FIRST FR II quasars (blue) and the re-scaled GRS 1915+105 (red)

2. During the 1 to 7 hours of major flare ejections, the time averaged power, $\langle Q \rangle$, and time averaged intrinsic radiative luminosity, $\langle L_{\text{bol}} \rangle$, are highly correlated.

Our estimates of L_{bol} are based on models where the main contribution is due to thermal Comptonisation of soft (cold ~ 0.2 keV) photons by hot (~ 20 -100 keV) electrons present in a so-called corona. The important parameters to estimate L_{bol} are kT_{inj} , kT_{e} , τ and the Comptonised normalization (see Section 4.2.2 of PR13). $\langle Q \rangle / \langle L_{\text{bol}} \rangle$ for each D is computed from the values in Tables 2 and 3 of PR13 for each flare. The solid line in Figure 4 is $\langle Q \rangle / \langle L_{\text{bol}} \rangle$ averaged over all the flares for each D. The dashed lines represent the standard deviation, $\pm\sigma$. The small dispersion argues strongly for an approximately constant ratio $\langle Q \rangle / \langle L_{\text{bol}} \rangle$ at each D. We assume that this is the case and the errors in the individual $\langle Q \rangle$ and $\langle L_{\text{bol}} \rangle$ are artifacts of imperfect data and our estimation methods. Equivalently, the uncertainty in $\langle Q \rangle / \langle L_{\text{bol}} \rangle$ for each D is σ .

There are two topologically distinct families of 3-D MHD simulations of accreting gas near rotating BHs that produce relativistic outflows. The limited flux simulations (LFS hereafter) evolve from the accretion of weak dipolar loops of magnetic flux of the same orientation from a finite torus of gas in the initial state (McKinney and Blandford 2009; Beckwith et al 2008b; Hawley and Krolik 2006; Krolik et al 2005). In these simulations, only the leading edge of the poloidal field accretes, so all the accreting large scale magnetic flux is of one sign. In the LFS, it is the accretion rate not the initial poloidal field strength that regulates the long term, large scale magnetic field strength near the black hole (and therefore the jet power) through ram pressure in the inner disk (private communication McKinney (2011) and Tchekhovskoy in Martinez-Sansigre and Rawlings (2011))). Physically, this situation might be considered a brief event of like sign large scale flux that accretes to the BH and is maintained near the BH by the dynamics of the accretion flow that is driven by a persistent MRI (magneto-rotational instability). The physical appeal of LFS is that memory of the initial state is erased and one finds a strong correlation between jet power and accretion rate in accord with the findings of PR13 that were noted above.

The second type of simulation is based on initial conditions that create MCAFs (magnetically choked accretion) and MADs (magnetically arrested accretion) (McKinney et al 2012; Tchekhovskoy et al 2011, 2012). A new topology emerges, islands of large scale magnetic flux perforate the disk, arresting the flow and suppressing the MRI induced dissipation in these regions. Thus, one would expect the luminosity to be suppressed compared to the LFS ¹. It was shown in PR 13 that ≈ 24 hours before an ejection L_{bol} is low and

¹Simulations of MADs that were reported in Punsly et al (2009) are generally subsonic and do not produce significant gas heating from shocks.

jetted emission is minimal, thus it is not an MCAF/MAD state (which have maximal jet efficiency). If an MCAF/MAD switches on to drive a major flare, it would imply that the switch-on of an MCAF/MAD jet is preferentially associated with an increase of X-ray luminosity to near the highest historic (non-transient) levels. But this circumstance is contradicted by the implications of our numerical simulations that radiative efficiency should be suppressed in MCAF/MADs (suppression was also noted in Sikora and Begelman (2013)). Since MCAF/MADs simulations do not appear to be representative of the high luminosity during major ejections, in this article we concentrate on the LFS that can be consistent with the dynamics of GRS1915+105.

In these simulations, the jet power, Q , is expressible in terms of accretion rate onto the BH, $\dot{M}c^2$. Thus, one can compare different simulations and one can compare to the observations if the radiative efficiency of the accretion flow due to viscous dissipation η_{th} , ($L_{bol} \equiv \eta_{th}\dot{M}c^2$) is known. In the numerical models, radiation effects are simulated by ad hoc cooling functions that are based on the local turbulent dissipation driven by MRI. In spite of a physically incomplete methodology for treating the emissivity of the accreting gas, the 3-D simulations of accretion disks in Penna et al (2010); Noble and Krolik (2009); Noble et al (2011) have been used to estimate a value,

$$1.0\eta_{NT} < \eta_{sim} \equiv \eta_{th} < 1.2\eta_{NT} , \quad (5)$$

where the range of results are expressed in units of η_{NT} , the value from (Novikov and Thorne 1973). The disk thickness in these simulations is in the range $0.05 < H/R < 0.2$. We consider this range of η_{sim} from equation (5) as a reasonable estimate for the η_{th} of the LFS in Figure 5 since they have a compatible range of disk thickness, $0.15 < H/R < 0.2$ (McKinney and Blandford 2009; Hawley and Krolik 2006). Furthermore, it was demonstrated in the simulations of Schnittman et al (2012) that even if the detailed radiative transfer results in the preponderance of disk luminosity being created by Compton scattering in a disk corona instead of thermal emission from the disk proper, η_{sim} is unchanged to first order and is still consistent with Equation (5). This is an important detail because X-ray spectra during the ejection of major flares do not exist, so the relative contributions of coronal and blackbody components are unknown. The simulations neglect radiation pressure in the disk, so η_{th} in Equation (5) might not be accurate (but see Szuszkiewicz et al (1996) who calculate $< 10\%$ change in η_{th} for the relevant Eddington rates).

Figure 5 compares the simulated data to the relationship depicted in Figure 4. The simulated data in the plot was presented and described elsewhere (see Punsly (2011) for details). The only change is that the data is normalized by $L_{bol} = \eta_{sim}\dot{M}c^2$ instead of $\dot{M}c^2$. The McKinney and Blandford (2009) $a/M=0.92$ simulation shows an event horizon jet as in Blandford and Znajek (1977). They note that $Q \approx 0.01\dot{M}c^2$ is similar to the 2-D solu-

tions reported in McKinney (2005). Thus, the spin dependent Q is given by equation (3) of McKinney (2005). This normalized jet power is plotted in green in Figure 5. The other event horizon jet data (collectively referred to as Event Horizon Jet (HK) in Figure 5) comes from Hawley and Krolik (2006); Krolik et al (2005) except for the raw data of Beckwith et al (2008a) for $a/M = 0.99$ and $a/M=0.998$ (Punsly 2011). The ergospheric disk jet data is from the simulations, KDE, KDH and KDJ from Hawley and Krolik (2006); Krolik et al (2005). The nature and strength of these jets was described in detail in Punsly et al (2009) and references therein. In order to remove the artificial variation induced by computational grids covering differing amounts of the ergospheric volume in different simulations, a theoretical fit to the data, "ergospheric disk with normalized inner boundary," (the red curve) was calculated in Punsly (2011). The fit was shown to exceed the KDE value because the inner boundary of the computational grid is farther from the event horizon in relative units (event horizon radius) than the other simulations. Thus it does not sample the entire ergosphere (which is critical for high BH spin in Boyer-Lindquist coordinates). The blue band in Figure 5 represents $\langle Q \rangle / \langle L_{\text{bol}} \rangle$ from Figure 4 corresponding to the viable range of D that is compatible with the scaling to FR II quasars in Figure 3, $10.7 \text{ kpc} < D < 11.0 \text{ kpc}$ (the dominant source of uncertainty is D). Agreement of the simulated data and observations is achieved for an ergospheric disk driven jet with a black hole spin, $a/M = 0.99$ or $a/M = 0.998$. The theoretical fit in red continuously samples a/M below 0.99 and indicates agreement for $a/M > 0.984$. This result agrees with the value of $a/M = 0.99 \pm 0.01$ that was estimated from the study of X-ray spectra of GRS 1915+105 (McClintock et al 2006; Blum et al 2009).

5. Conclusion

In this article, the long term and episodic behaviors of L_{bol} and the power of superluminal ejections in GRS 1915+105 were compared and contrasted with FR II quasars under the assumption of scale invariance of BH accretion systems. The results of Section 3 indicate that re-scaling L_{bol} of GRS 1915+105 to a typical range of L_{bol} of FR II quasars yields a consistent distribution of \overline{Q} only if $D > 10.7 \text{ kpc}$ - otherwise the total energy emitted in the superluminal major ejections is too small. Physically, this constraint on the distance is equivalent kinematically to a Doppler factor < 0.48 and a bulk Lorentz factor > 3.5 for the approaching plasmoids. Comparison of the GRS 1915+105 data with the results of different 3-D numerical simulations of the BH accretion indicate that GRS 1915+105 is compatible with both numerical models and re-scaling to FR II quasars if the numerical models contain an ergospheric disk jet and if $a/M > 0.984$, in agreement with observational results obtained by different groups and methods. If the analogy with FR II quasars is robust and scale

invariance is relevant to astrophysical BHs, the results obtained for GRS 1915+105 may imply that typical radio loud quasars also harbor rapidly spinning BHs.

We would like to thank Igor Igumenshchev for many in-depth discussions on magnetically arrested accretion. We are also grateful to Matt Malkan for sharing his insight into high Eddington rate accretion and the effects on the geometry and efficiency of accretion disk models. JR acknowledges partial funding from the European FP7 grant agreement number ITN 215212 “Black Hole Universe”, and the hospitality of ESO (Garching, Germany) where part of this work was done.

REFERENCES

- Beckwith, K., Hawley, J., Krolik, J. 2008, MNRAS 390 21
- Beckwith, K., Hawley, J., Krolik, J. 2008, ApJ 678 1180
- Belloni, T. et al 1997, ApJL 488 109
- Blandford, R. and Znajek, R. 1977, MNRAS 179 433
- Blum, J. et al 2009, ApJ 706 60
- Dhawan, V., Mirabel, I.F., Rodriguez, L. 2000, ApJ 343 373
- Done, C., Wardzinski, G., Gierlinski, M. 2004, MNRAS 349 393
- Fender, R. et al, 1999, MNRAS 304 865
- Hawley, J., Krolik, K. 2006, ApJ 641 103
- Krolik, J., Hawley, J., Hirose, S. 2005, ApJ 622 1008
- Martnez-Sansigre, A., Rawlings, S. 2011, MNRAS 414 1937.
- McClintock, J. et al 2006, ApJ 652 518.
- McKinney, J. 2005, ApJL 630 5
- McKinney, J., Blandford, R. 2009, MNRAS Letters 394 126
- McKinney, J. and Gammie, C. 2004, ApJ 611 977
- McKinney, J., Tchekhovskoy, A., Blandford, R. 2012, MNRAS 423 3083

- Miller-Jones, J. et al 2005, MNRAS 363 867
- Mirabel, I.F., Rodriguez, L. 1994, Nature 371 46
- Muno, M., Morgan, E, Remillard, R. 1999, ApJ 527 321
- Noble, S., Krolik, J. 2009, ApJ 692 411
- Noble, S., Krolik, J., Schnittman, J, Hawley, J. 2011, ApJ 743 115
- Novikov, I. and Thorne, K. 1973, in *Black Holes: Les Astres Occlus*, eds. C. de Witt and B. de Witt (Gordon and Breach, New York), 344
- Penna, R. et al 2010, MNRAS 408 752
- Punsly, B. 2005, ApJL 623 9
- P12 Punsly, B. 2012, ApJ 746 91
- Punsly, B. 2011, ApJL 728 17
- Punsly, B., Igumenshchev, I. V., Hirose, S. 2009, ApJ 704 1065
- PR13 Punsly, B., Rodriguez J. 2013, ApJ 764 173
- Punsly, B., Zhang, S. 2011, ApJL 735 3
- Reed, B. 1989, Am. J. Phys. 57 642
- Schnittman, J, Krolik, J., Noble, S. 2012, submitted to ApJ
<http://xxx.lanl.gov/abs/1207.2693>
- Sikora, M., Begelman, M. 2013, ApJL 764 24
- Szuskiewicz, E., Malkan, M., Abramowicz, M 1996, ApJ 458 474
- Tchekhovskoy, A., Narayan, R. and McKinney, J. 2011, MNRAS Letters 418 79
- Tchekhovskoy, A.,McKinney, J. 2012, MNRAS Letters 423 55
- Willott, C., Rawlings, S., Blundell, K., Lacy, M. 1999, MNRAS 309 1017

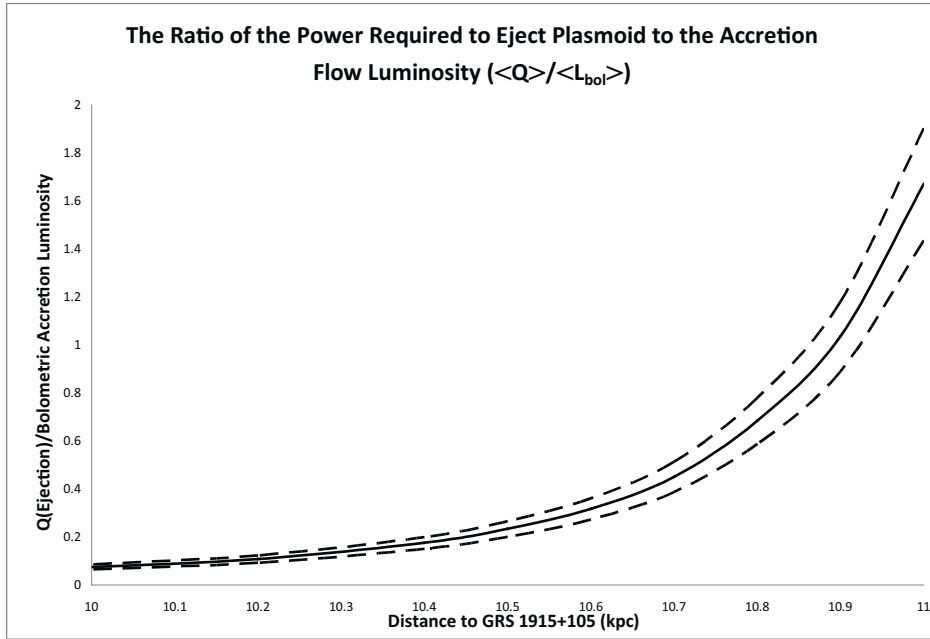


Fig. 4.— $\langle Q \rangle / \langle L_{\text{bol}} \rangle$ as a function of the assumed distance, D , to GRS 1915+105.

Jet Power of Major Flares Compared to Limited Flux Simulations

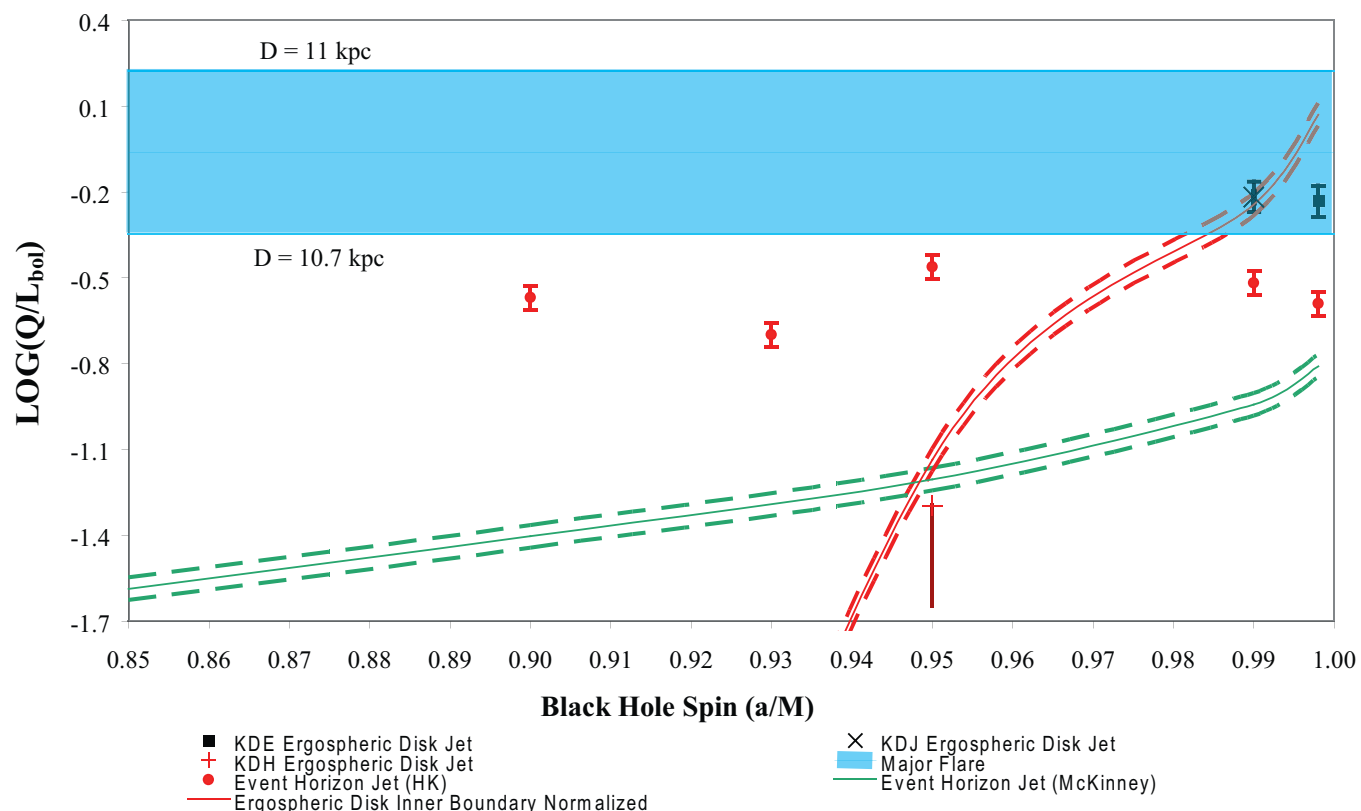


Fig. 5.— The logarithm of "jet power/ L_{bol} " in the numerical simulations compared to $\log[\langle Q \rangle / \langle L_{\text{bol}} \rangle]$ for major flares in GRS 1915+105 based on Figure 4. The limited range of $10.7 \text{ kpc} < D < 11 \text{ kpc}$ indicated by the blue band, is the range of distance for which GRS 1915+105 can be considered a scaled down FR II quasar. The error bars and the range of uncertainty on the curves (the dashed curves) are based on the spread in Equation (5)